The effect of spectral albedo on amorphous silicon and crystalline silicon solar photovoltaic device performance

Rob W. Andrews, Joshua Pearce

The Effect of Spectral Albedo on Amorphous Silicon and Crystalline Silicon Solar Photovoltaic Device Performance

Rob W. Andrews[a] and Joshua M. Pearce[b,*]

[a] Department of Mechanical and Materials Engineering, Queen's University, Canada
[b] Department of Materials Science and Engineering and Department of Electrical and Computer Engineering, Michigan Technological University, USA

Abstract

In this paper the theory of mismatch factor of the terrestrial solar spectrum is extended to more accurately represent the irradiance available to specific types of photovoltaic (PV) materials from surface albedo. Using spectra derived from the SBDART radiative transfer model, the effects of a spectrally responsive albedo are illustrated by the differences between the spectrally weighted albedo of hydrogenated amorphous silicon (a-Si:H) and crystalline silicon (c-Si)-based PV technology compared to traditional spectral-integrated albedo predictions. In order to quantify this effect for varying representative spectra, spectra for cloud optical thicknesses from 0-150 were investigated. Grass was found to be a poor reflector in the a-Si:H spectral response range with a spectrally responsive albedo of 0.08-0.07 as cloud optical thickness increased from 0-150, whereas snow is a good reflector with a relatively constant spectrally responsive albedo of 0.94 as cloud optical thickness increased from 0-150. For c-Si PV systems the spectrally responsive albedo for snow and grass were found to be 0.87-0.91 and 0.24-0.15 as cloud optical thickness increased from 0-150, respectively. These values can be compared to the albedo typically predicted from spectral integration relative to an AM1.5 spectrum of 0.78 for snow and 0.23 for grass. On a yearly basis, the use of improper albedo values can lead to an under-prediction of system yields of 0.04%, 2.4%, and 10.5% for systems at 25°, 40°, and 90° tilt from the horizontal, respectively. This can lead to improper PV systems optimization and masking of other loss mechanisms. The results of this study have implications for both solar systems evaluation and systems design, and supports further research on tailoring PV technologies specifically to the climate and geographic location where they are deployed.

Keywords: albedo, PV, amorphous silicon, crystalline silicon, reflection, spectral mismatch factor, spectral albedo

1. Introduction

The optimal design of a photovoltaic (PV) array relies upon accurate performance predictions of the system and a thorough understanding of the electrical and environmental factors that effect systems performance (Thevenard et al., 2010). Two of the largest PV technologies being implemented worldwide include crystalline silicon c-Si and hydrogenated amorphous silicon-based (a-Si:H). These two technologies are compared in this study due to their wide adoption, and the large difference in their spectral responsivity. PV systems utilizing a-Si:H have been proven through a variety of successful projects to be a low-cost solution with minimized life cycle ecological impacts for implementing PV systems throughout the world (Schwabe and Jansson, 2009; Jardine et al., 2001; Pearce and Lau, 2002), however its output is generally under-predicted by conventional techniques developed for crystalline Si (c-Si)-based PV technology. This is due mainly to

Nomenclature

	Superscripts
$G(\lambda)$	Spectral Solar irradiance $(W/m^2/nm)$
$SR(\lambda)$	Spectral module response $(A/W/nm)$
$A(\lambda)$	Spectral reflectivity function $(1/nm)$
E	Solar irradiance (W/m^2)
I	Current (A)
M	Mismatch Factor
R	Geometric translation factor
F	View factor
α	Reflectivity
θ	module angle from horizontal

	Subscripts
t	Total
b	Beam
d	Diffuse
a	Albedo
p	In-Plane
h	In the horizontal plane
SI	Spectrally integrated and normalized
SR	Spectrally weighted and normalized
ref	Relating to ASTM G-173 AM1.5

*1400 Townsend Drive Houghton, MI 49931-1295 906-487-1466
Email address: pearce@mtu.edu (Joshua M. Pearce)

1. Superior a-Si:H temperature coefficient (Schwabe and Jansson, 2009; Carlson et al., 2000)

2. Use of broadband integrated solar information collected from pyranometers

The latter effect can directly introduce errors up to 20% in the prediction of a-Si:H PV system yearly output due to the inability of broadband irradiance measurements to properly account for variations of the global spectrum. The effects of temperature and spectral dependence in addition to possible seasonal thermal annealing of the a-Si:H can also lead to seasonal variations in the module performance which must be accounted for in order to ensure proper production estimates from these devices (Pathak et al., 2012; Rther et al., 2002; Rther and Livingstone, 1995; Gottschalg et al., 2004; Hirata and Tani, 1995; Merten and Andreu, 1998; Betts et al., 2003b; Williams et al., 2003). Similar spectral effects are seen in c-Si PV systems, however to a lesser degree due to their smaller bandgap that provides a larger spectral range (Williams et al., 2003; Simon and Meyer, 2011; Bamshad Houshyani, 2006).

These spectral errors originate from the assumption that all irradiance collected by the device has the same spectral distribution as the ASTM G173 AM1.5 standard (ASTM, 2008). Because there are daily, locational and seasonal shifts in the spectral distribution of incident radiation at ground level (Gottschalg, 2003), this is generally not a valid assumption and leads to modelling errors as improper spectral weighting is utilized to calculate the module response to irradiance. In order to account for these spectral effects, multiple methods have been suggested. If spectral information is not available for the site, a common methodology is to utilize experimental data to generate an empirical correlation based on air mass to determine a spectral correction coefficient (King et al., 2004). Another methodology is to generate a clear-sky spectra using a radiative transfer model tuned to the atmosphere of the location where modules are installed, and to utilize this spectra as a substitute for measured values (Nann and Emery, 1992; Gueymard, 2001, 2005).Neither of these methodologies account for cloud cover, but are generally considered accurate over large time scales.

If spectral information is available, either through measurements or modelling, it can be quantified through a variety of metrics. A common quantification is the use of a Useful Fraction (UF), which is the fraction of spectral irradiance integrated up to the band gap of the technology being considered, divided by the total integrated irradiance (Hirata and Tani, 1995). Another common measure is the Average Photon Energy (APE), which indicates the median photon energy value of a spectrum and is a technology independent measure of the spectral distribution. For example, the APE of the AM 1.5G spectrum is 1.6 eV (Betts et al., 2003b). In order to better quantify the useful spectrum available for a specific technology, the theory of UF is modified by convolution of the spectrum to the spectral response of a chosen technology, creating the Weighted Useful Fraction (WUF) (Simon and Meyer, 2011).

As an extension to these approaches, the level of useful irradiance is translated to an equivalent scaled AM1.5 spectrum that would produce the same level of useful irradiance. This is performed utilizing a Mismatch Factor (MMF) that is described in IEC 60904-7 (IEC, 2008) and which has been discussed in detail in (IEC, 2008; King and Hansen, 1991; Whitaker and Newmiller, 1998) . The general formulation of mismatch factor is calculated as :

$$
\begin{aligned}
M &= \frac{\int_{\lambda_i}^{\lambda_f} SR(\lambda)G_{tot}(\lambda)d\lambda}{\int_{\lambda_i}^{\lambda_f} SR(\lambda)G_{ref}(\lambda)d\lambda} \frac{\int_{\lambda_i}^{\lambda_f} G_{ref}(\lambda)d\lambda}{\int_{\lambda_i}^{\lambda_f} G_{tot}(\lambda)d\lambda} \\
&= \frac{I_t}{I_{ref}} \frac{E_{ref}}{E_t}
\end{aligned}
\tag{1}
$$

The integration limits of this equation are $\lambda_i = 250nm$, $\lambda_f = 2500nm$ and this convention is used for the entire study. There are some more commonly used parametrizations of this equation, such as those applied in the Sandia PV performance model as a function of Air Mass (King et al., 2004; Andrews et al., 2012), and in other cases the mismatch factor is assumed to be unity with the assumption that all spectra are equivalent to the AM1.5 spectrum. Thus, spectral correction to determine effective AM1.5 scaled irradiance (E_{Spec}) is applied as shown in Equation 2, where the spectral modifier (in this case M) is applied to all radiation components equally:

$$
E_{spec} = M_{glob}(R_b \int_{\lambda_i}^{\lambda_f} G_b(\lambda)d\lambda + F_{sky} \int_{\lambda_i}^{\lambda_f} G_d(\lambda)d\lambda + \dots
$$
$$
\dots + F_{ground}\alpha \int_{\lambda_i}^{\lambda_f} G_{tot}(\lambda)d\lambda)
\tag{2}
$$

However, as can be seen in Figure 1, which shows the beam, diffuse and albedo radiation for two days with the same value of horizontal down welling integrated broadband irradiance, the distribution of irradiance over the three components of radiation is not equal between a clear, sunny day at high air mass and a cloudy day at low air mass.

Thus, it is clear to make highly accurate predictions of PV performance, a separate spectral modifier should be applied to each component of the radiation as shown in equation 3.

$$
E_{spec} = M_b R_b \int_{\lambda_i}^{\lambda_f} G_b(\lambda)d\lambda + M_d F_{sky} \int_{\lambda_i}^{\lambda_f} G_d(\lambda)d\lambda + \dots
$$
$$
\dots + M_a F_{ground}\alpha \int_{\lambda_i}^{\lambda_f} G_{tot}(\lambda)d\lambda
\tag{3}
$$

Previous work has comprehensively studied the effects of the spectral shift of direct and diffuse radiation
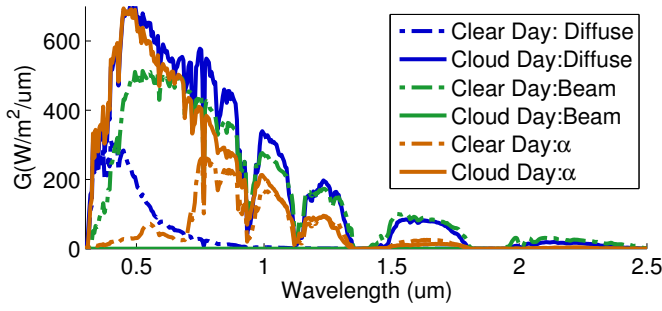
Figure 1: Spectrum generated for two days with a global down welling irradiance of 400 W/m^2. 'Clear day' has a Solar Zenith Angle(SZA) of 67°, cloud optical depth of 0, and a snow surface albedo.'Cloudy day' has a SZA of 48°, cloud optical thickness of 8 and a grass surface albedo.

components on PV module performance (Rther et al., 2002; Rther and Livingstone, 1995; Gottschalg et al., 2004; Hirata and Tani, 1995; Merten and Andreu, 1998; Betts et al., 2003b; Williams et al., 2003). Therefore the purpose of this paper is to extend the analysis of spectral response on PV performance to determine the effects of spectral distribution on the albedo for PV devices and to suggest best practices for design using these albedo values.

The useful fraction for amorphous silicon is calculated using a band gap of 1.7eV giving an integrated spectral range of 300nm-780nm (Gottschalg et al., 2004). This is a significantly narrower integrated range compared to c-Si PV (300nm-1100nm) (Nann and Emery, 1992), which has a band gap of 1.1eV, and to the response of a typical pyranometer (200nm-3600nm) (Gottschalg et al., 2004). Because the response of a-Si:H only covers a small fraction of this range, differences in the spectrum will have an amplified effect on the performance of an a-Si:H PV cell when compared to a c-Si PV devices, which covers a much wider spectral range. These effects have been widely documented (Rther et al., 2002; Rther and Livingstone, 1995; Gottschalg et al., 2004; Hirata and Tani, 1995; Merten and Andreu, 1998; Betts et al., 2003b; Williams et al., 2003) and is one of the reasons generally attributed to the claims that a-Si:H PV modules will produce more energy per rated power than c-Si PV modules when deployed in real world operating conditions(Williams et al., 2003; Simon and Meyer, 2011). This paper will extend that analysis to investigate the effects of albedo spectral mismatch and spectrally responsive albedo on the prediction and modelling of PV device performance.

2. Methodology

2.1. Spectrally responsive albedo calculation

Spectrally-integrated albedo, α_{SI}, is traditionally defined as the ratio of reflected radiation to the radiation

from the sky dome, which can be represented in integral form as:

$$\alpha_{SI} = \frac{\int_{\lambda_i}^{\lambda_f} A(\lambda)G(\lambda)d\lambda}{\int_{\lambda_i}^{\lambda_f} G(\lambda)d\lambda} = \frac{E_a}{E_t} \qquad (4)$$

Where A(λ) is the normalized reflectance as a function of wavelength. A(λ) is traditionally considered to be a constant value (A) across the spectrum, in which case $\alpha_{SI} = A$. However, this formulation does not take into account the difference in mismatch factor between the reflected spectra and the global spectrum. Therefore, a separate mismatch factor, as applied in Equation 1 must be applied to α_{SI} as shown in Equation 5

$$M_a \alpha_{SI} = \frac{I_a}{I_{ref}} \frac{E_{ref}}{E_a} \frac{E_a}{E_t}$$
$$= \frac{E_{ref}}{I_{ref}} \frac{I_a}{E_t} \qquad (5)$$

This correction can be generalized by looking at the difference between the global and albedo irradiance mismatch factors. In this case, the important quantity is the albedo mismatch factor *relative* to the global mismatch factor. It is also important to note that in the case that a mismatch factor is not explicitly defined, M_{glob} *still exists* however the implicit assumption being made is that $M_{glob} = 1$, and in this case it is still desired to determine the mismatch factor of albedo relative to global irradiance. Therefore, Equation 5 is simplified by normalizing by M_{glob} which eliminates the dependence on the reference spectrum and includes the relative difference between an arbitrary global mismatch factor and the albedo mismatch factor. This gives a new albedo definition of the Spectrally Responsive albedo (α_{SR}):

$$\alpha_{SR} = \frac{M_a \; \alpha_{SI}}{M_{glob}}$$
$$= \frac{\frac{E_{ref}}{I_{ref}} \frac{I_a}{E_t}}{\frac{I_t}{I_{ref}} \frac{E_{ref}}{E_t}}$$
$$= \frac{I_a}{I_t}$$
$$= \frac{\int_{\lambda_i}^{\lambda_f} SR(\lambda)A(\lambda)G(\lambda)d\lambda}{\int_{\lambda_i}^{\lambda_f} SR(\lambda)G(\lambda)d\lambda} \qquad (6)$$

It is important to note that both Equation 5 and Equation 6 are valid methods of acconting for the spectrally responsive albedo, and that Equation 5 should be used if seperate mismatch factors are utilized for each component, and Equation 6 should be used if a global mismatch factor is being applied (or in the case that none is applied). This paper will utilize Equation 6 due to its general applicability to a broad range of modelling techniques.

2.2. Spectral Modelling

Because of the expense of measurement equipment, the availability of measured full spectrum data is limited, and as such many simulations programs have been developed that can reproduce typical spectral distributions for incident light based upon user defined inputs for variables. Some available programs are SMARTS2, ASPIRE, SBDART, MODTRANS, RRTM SW and SEDES2 (Gueymard, 2005; Betts et al., 2003a; Houshyani, 2007; Ricchiazzi et al., 1998; Clough et al., 2005). The simulations package chosen for this study is SBDART because of the simplicity of inputs and the ability to model atmospheric cloud layers (Ricchiazzi et al., 1998), in addition to its previously validated accuracy versus MODTRANS and ground based measurements (J.C Barnard and D.M Powell, 2001; Barnard and Powell, 2002; Gueymard, 2008). Cloud layers are accounted for in this model through the cloud optical thickness and altitude. Cloud optical thickness (δ_{cloud}) is a non-dimensional characteristic of the transmissivity of the cloud layer and is defined as the natural logarithm of the ratio of integrated radiation at the top of the cloud to integrated radiation below it (Goosse H. et al., 2011).The average cloud optical thickness for a region is dependant on latitude and at a latitude of 45 degrees the average cloud optical thickness is 15 with instantaneous optical thicknesses of up to 150 being possible for stratus and nimbostratus clouds (Tselioudis et al., 1992). The horizontal downwelling spectrum is calculated with SBDART, using the input parameters shown in Table 1.

Table 1: Atmospheric parameters for modelled spectrum

Solar Spectrum	LOWTRAN 7 Spectrum
Solar Zenith Angle	48.1°
Surface Albedo	Snow or Grass
Column Water Vapour	0.854 (g cm)
Total Ozone	0.403 (atm-cm)
Atmospheric Profile	Mid-Latitude Winter

The generated spectrum is meant to represent a realistic spectrum that could be seen by a PV device, generated at an air mass of 1.5. This spectrum does not match with AM1.5G as defined by ASTM G173-03, as the atmospheric conditions are different and the SBDART code generates horizontal downwelling irradiance, rather than the 37° in plane irradiance defined in AM1.5G. This spectrum was chosen to be a general, realistic spectrum and the investigation of the air mass dependence on α_{SR} is left for future work.

Figure 2 shows two global solar spectra generated in SBDART that are representative of a clear sky and a cloudy sky, with clouds of optical thickness((δ_{cloud})) 50, for an air mass of 1.5 (solar zenith angle of 48.2°). Overlaid on this data is the spectral response

characteristic of typical a-Si:H and c-Si PV cells, defined by (Kenny et al., 2006), and the non dimensional albedo of grass and snow (Gardner and Sharp, 2010).
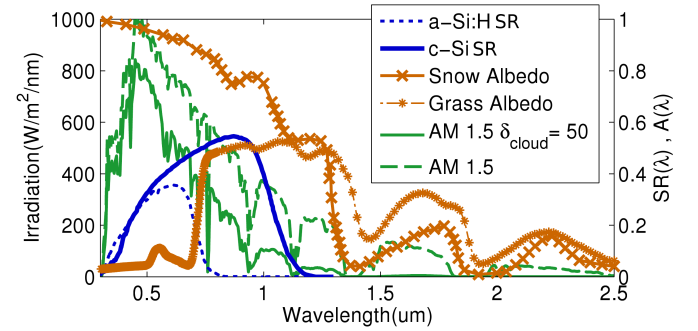

Figure 2: Effect of cloud cover on the AM 1.5 spectrum generated by SBDART. Overlaid is the spectral response curve of a-Si:H and c-Si PV devices (Kenny et al., 2006), the albedo of snow (Gardner and Sharp, 2010) and the albedo of green grass (Baldridge et al., 2009).

It can be seen in Figure 2 that the introduction of cloud layers tends to shift the spectrum towards the UV, increasing the APE of the spectrum. On the other hand, in the case of an increase in air mass (AM) or introduction of atmospheric turbidity will tend to cause a shift towards the IR, decreasing the APE of the radiation.

The albedo of grass and snow shown in Figure 2 are also highly spectrally dependent. Snow in particular is interesting as its spectrally responsive albedo can change dramatically over the course of a winter. The major factors that effect the albedo of snow are solar zenith angle, effective grain size and soot. For a full description of the variability of albedo with these factors, Warren (Warren, 1972) and Gardner and Sharp (Gardner and Sharp, 2010) provide a very detailed analysis. In addition, snow has been shown to be an anisotropic reflector, meaning that the reflection will tend to be forward biased, as opposed to completely diffuse.

The albedo information for grass is taken from the ASTER Spectral Library data provided by the NASA Jet Propulsion Laboratory (Baldridge et al., 2009).

2.3. Effects of Albedo on PV Performance

In order to determine the importance of properly accounting for albedo, its effects on PV performance should be understood. For simplicity, the isotropic sky model (Duffie and Beckman, 1991) is utilized to identify the irradiance on an inclined surface. Considering only the radiation emanating from the sky, the isotropic model gives the total in-plane irradiance, E_p, as:

$$E_p = E_h b R_b [1 - F_B] + E_h (1 - b) \frac{1 + \cos(\theta)}{2} [1 - F_D] \quad (7)$$

Where I_h is the total horizontal radiation, b is the ratio of direct beam to global horizontal radiation, R_b is the

geometric translation factor defined by Duffie and Beckman (Duffie and Beckman, 1991) and θ is the angle of inclination of the module from horizontal. F_B, F_D, and F_A are terms which account for reflectance losses due to the angle of incidence of irradiation, as defined in (Martin and Ruiz, 2001). For beam radiation, an angle of incidence of 40° is assumed. Assuming an unobstructed view factor with the surroundings, the radiation coming from the ground, E_a, is given by:

$$E_a = E_h \alpha \frac{1 - \cos(\theta)}{2}[1 - F_A] \qquad (8)$$

Where α represents the albedo of the surface. For the case of this study, this value can either be the spectral-integrated, spectral-weighted, or AM1.5 equivalent albedo depending on the quantity being investigated. Combining equations 7 and 8 for the two sources, the ratio of albedo radiation to total in-plane radiation is given as:

$$\frac{E_a}{E_p} = \frac{\alpha \frac{1-\cos(\theta)}{2}[1 - F_A]}{bR_b[1 - F_B] + (1 - b)\frac{1+\cos(\theta)}{2}[1 - F_D]} \qquad (9)$$

Therefore relative effect of albedo is dependant on module angle, spectral-integrated albedo, diffuse ratio and the geometric factor.

3. Results

3.1. Derivation of spectrally responsive albedo

Numerical simulations were run to calculate the SR weighted global (G_{G-SR}) and reflected (G_{A-SR}) radiation components for snow and grass surfaces in cloudy and clear conditions for c-Si and a-Si:H PV modules. The results of these simulations, shown at cloud optical thicknesses of 0 and 150, can be seen in Figures 3- 6.

Figure 3 shows the spectral-weighted global and reflected radiation for clouds of optical thickness 50, and green grass surface. In addition, the spectral reflectance of green grass from the ASTER library (Baldridge et al., 2009) is shown in Figures 3 and 4. In Figure 4 the spectral-weighted global and reflected radiation is shown for the same green grass surface with clear skies.

Figure 5 provides the spectral-weighted global and reflected radiation for clouds of optical thickness 50, and reflectance for snow at a fine grain size and solar zenith angle of 60°.Figure 6 shows the same results for clear skies.

In order to study the sensitivity of the spectrally responsive albedo to cloud cover for the two technologies investigated, a series of simulations were run at a range of cloud optical thicknesses and the spectrally responsive albedo (α_{SR}) was calculated for c-Si, a-Si:H, as shown in Equation 6. The results of this can be seen in Figure 7 and Figure 8 for grass and snow, respectively.

It is interesting to note that the spectrally integrated estimate for snow albedo sees a steep increase with
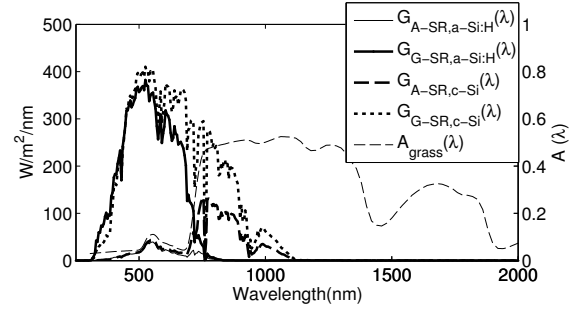
Figure 3: Spectral-weighted global and reflected radiation for clouds of optical thickness 50, and green grass surface. Overlaid is the spectral reflectance of green grass from the ASTER library (Baldridge et al., 2009).
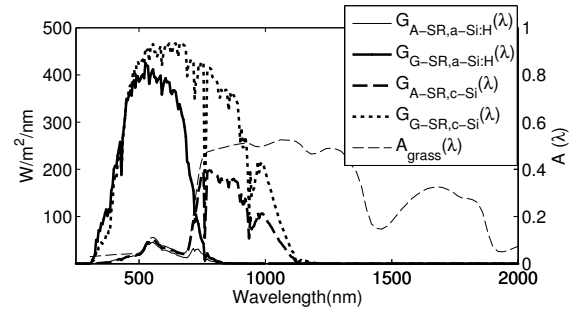
Figure 4: Spectral-weighted global and reflected radiation for clear skies, and green grass surface. Overlaid is the spectral reflectance of green grass from the ASTER library (Baldridge et al., 2009).
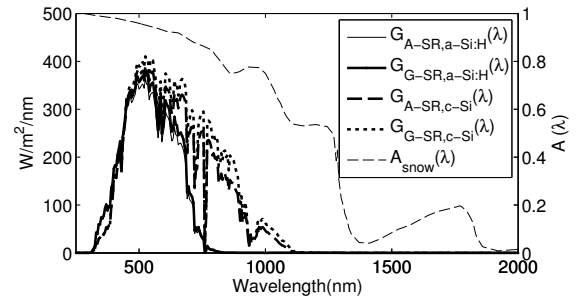
Figure 5: Spectral-weighted global and reflected radiation for clouds of optical thickness 50, and reflectance for snow at a fine grain size and solar zenith angle of 60. Overlaid is the spectral reflectance of snow (Wiscombe and Warren, 1980).
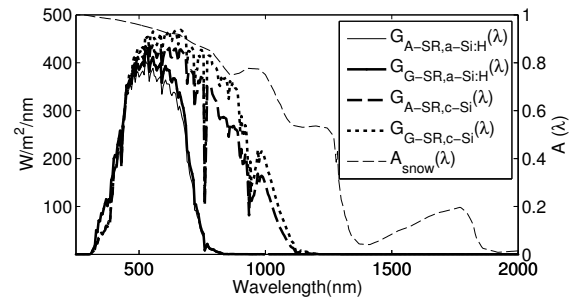
Figure 6: Spectral-weighted global and reflected radiation for clear skies, and reflectance for snow at a fine grain size and solar zenith angle of 60. Overlaid is the spectral reflectance of snow (Wiscombe and Warren, 1980).
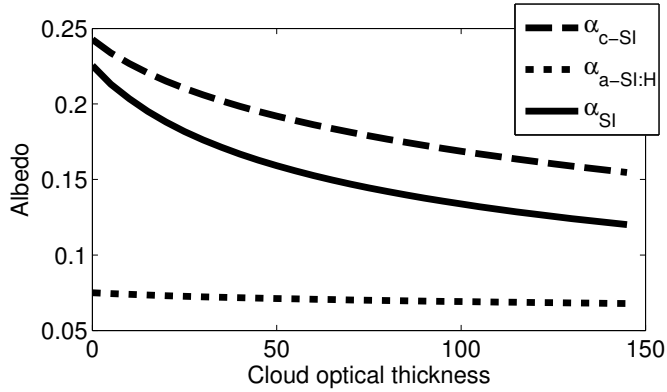
Figure 7: Sensitivity of the albedo of grass as a function of cloud optical thickness. The curves shown represent the spectrally responsive albedo for a-Si:H and c-Si technologies, and spectral-integrated albedo.
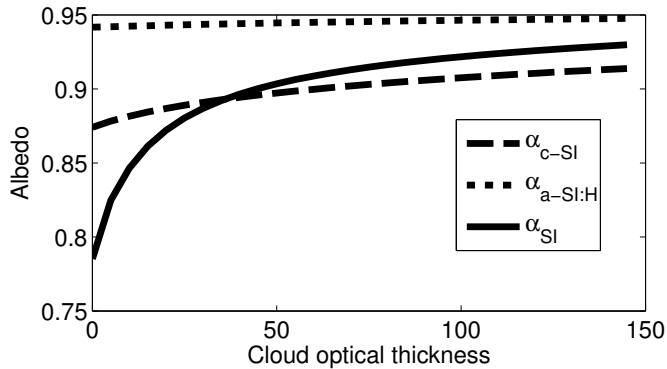

Figure 8: Sensitivity of the albedo of snow as a function of cloud optical thickness. The curves shown represent the spectrally responsive albedo for a-Si:H and c-Si technologies, and spectral-integrated albedo.

lead to sub-optimal designs and a masking of other loss mechanisms. Thus, a comparison is made between predicted module power using traditional albedo values, and the spectrally responsive albedo values suggested in this paper. In order to visualize the effects of albedo on PV module performance, Equation 9 was solved for two typical installation cases, representing a ground mounted PV array at 40 degree inclination, and module installed at 90 degrees (for example a Building Integrated PV (BIPV) faade installation). Both cases were analysed on a clear day(b=0.9) at 48° zenith angle with snow albedo. This resulted in a curve for each installation representing the ratio of albedo irradiation to in-plane irradiation $\frac{E_a}{E_t}$ shown in Figure 9. The absolute difference between the ratio $\frac{E_a}{E_t}$ for traditional and spectrally responsive albedos is equivalent to the model error introduced due to this assumption. From Figure 9 it can be seen that the use of
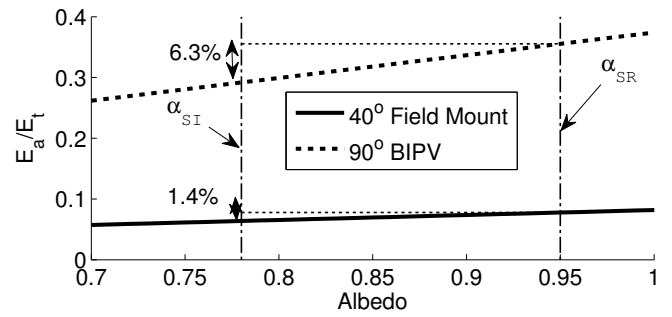

Figure 9: Comparison of albedo ratio for the spectral-integrated(α_{SI}) and spectrally responsive (α_{SR}) albedo with Rb=1.2 for two typical installations. The spectrally responsive albedo predicted for an amorphous silicon module on a clear day at a zenith angle of 48 is .95. Compared with the spectral-integrated value of 0.78, (typical PV modelling uses a value between 0.7-0.8), this corresponds to a modelled power error of 1.6% for a 40 field mount and 7% for a vertical (e.g. BIPV) module.

a spectral-integrated albedo of 0.78, as has been done previously (Whitaker and Newmiller, 1998), as opposed to the spectrally responsive albedo of 0.95 can lead to errors of 1.6% and 6.7% for 40° and 90° modules respectively. This represents only one possible combination of solar angle and beam ratio. In reality, the effects of albedo will change dramatically based on atmospheric conditions, and the next section shows the effect of the application of α_{SR} to a full year.

3.3. Effects on PV Module Energy Performance

In order to demonstrate the importance of the proper handling of albedo for varying forms of PV systems, an example is shown which takes insolation and snowfall data from 2011 to show the relative errors incurred through the use of spectrally integrated albedo. For this example, it was assumed that the spectrally responsive albedo value always corresponds to the clear sky value at AM1.5, the modules had an unobstructed view factor to

increasing cloud optical depth. As previously mentioned, the effects of increased cloud absorption are biased towards the near-infra-red side of the spectrum. Therefore, as cloud optical depth increases, the average photon energy of the spectrum shifts towards the ultraviolet. Because snow albedo is also biased towards the ultraviolet, the removal of the infra-red component of incoming irradiation as cloud optical thickness increases causes the ratio of reflected irradiation to cloud attenuated irradiation to increase, thus increasing the albedo. Because the spectral response of both devices studied does not extend far into the near infra-red, the effects of this infra-red attenuation are not seen to the same extent as the spectrally integrated case.

3.2. Effects on PV Module Power Performance

The use of the more realistic albedo can change predictions about module power output, and understanding the magnitude of these changes is important as improper predictions of performance can

the ground, and albedo was assumed to be completely non-specular. The modules are assumed to be amorphous silicon, with a spectrally responsive albedo of 0.94 in periods of snowfall and 0.07 when grass is present. The spectrally integrated albedos were assumed to be 0.78 and 0.23 for periods of snowfall and grass, respectively. Finally, the spectrally responsive in-plane insolation is assumed to be proportional to module AC energy yield.

For periods when there was snow present on the ground, the snow albedo term was used, otherwise a green grass albedo was applied. Three systems were simulated, with module tilt angles from horizontal of 25°, 40°, and 90°. The insolation in the plane of the array was calculated using equations 7 and 8, and the resultant difference in monthly insolation between the spectrally integrated ($E_{\alpha_{SI}}$) and spectrally responsive ($E_{\alpha_{SR}}$) albedos is shown in Figure 10.
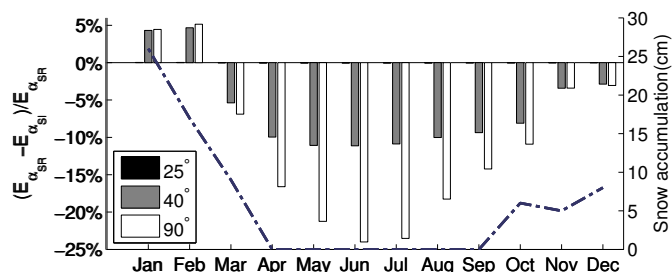

Figure 10: Monthly errors in insolation prediction arising from the use of α_{SI} instead of the α_{SR} presented in this paper. It can be seen that output will be over-predicted in periods where grass is present, and under-predicted when snow is present. On a yearly basis, the error is -0.04%, -2.4% and -10.5% for 25°, 40°, and 90° respectively.

In the case of the 90° module, production is at a minimum during the summer months due to the high angle of incidence of beam irradiation. However, because the module has a large view factor with its surroundings, and because the magnitude of global irradiance is high, albedo can have a large effect on the performance of this system. Therefore, incorrect handling of the albedo component of this system can have large effects on its overall performance. In contrast, the effects on a system with a 25° tilt is small enough to be negligible, and the proper use of spectrally responsive albedo in this case is not as critical.

4. Discussion

The results show that the spectrally responsive albedo received by a PV device is dependant on the spectral nature of the ground covering in the area, the band gap of the PV material, and the ambient spectrum. For single-junction a-Si:H-based PV it is clear that this spectrally responsive albedo can be higher than expected for the case of snow and lower than expected for the case of grass.

The practical effect of this is two-fold. First, in a northern climate albedo will be over estimated for the summer and under estimated in the winter thus the system orientation will not be optimized to correctly take advantage of the greatest combination of irradiance. It should be noted that for a fixed module geometry at moderate angles, the effect integrated over an entire year will be small, due to the small relative decrease in the summer and a relative increase in the winter averaging. However, in the case of a seasonal tilt or high-tilt (such as BIPV) system it can be seen in Figure 10 that the effects on predicted energy yield can be large.

In addition, in the winter time the under-prediction of albedo will tend to mask other forms of losses that may occur. For example, if the modules are covered with snow, production will decrease. However, in the periods where the modules are clear, they will be producing more energy than predicted by models relying on spectral-integrated albedo, which will be utilized to evaluate system performance. Therefore, over larger time scales being monitored, the losses due to snowfall may be masked by increased albedo.

This investigation accounted for the situation where the sun was at an angle of 48.1°, giving an air mass of 1.5. The results of the spectral mismatch will change over the course of the day and seasons, as the spectrum will shift towards the infra-red at higher air mass, and the ultraviolet at lower air mass. Thus, the purpose of this paper was not to define albedo spectral mismatch and albedo factors for all operating conditions, but rather to make the case for an alternative methodology to properly account for all forms of radiation incident on the surface of a photovoltaic system. Therefore, it is recommended to treat the spectral mismatch for each component of the radiation separately, and to assess the albedo based on the spectral reflectivity and spectral response of the reflecting surface and module.

5. Conclusions

This paper has demonstrated a more rigorous method of treating the ambient albedo for PV, which overcomes limitations of prior techniques that limited the optimization of systems in real world conditions. Spectrally responsive albedo was defined as the reflectivity of a surface convoluted with the spectral response of the module technology. This definition for spectrally responsive albedo can be integrated into most common modelling methodology, and accounts for the difference in mismatch factor between incident global and albedo irradiance.

Because of the spectral nature of the reflecting surface, the spectrally responsive albedo was shown to be different than the spectral-integrated value that is typically used for performance predictions and systems design. In the specific case of single-junction a-Si:H PV it was found that

grass is a poor reflector in the range of response for a-Si:H, and that its spectrally responsive albedo is 0.08-0.07, decreasing as cloud cover increases, whereas snow is a very good reflector in the range of response of a-Si:H and has an spectrally responsive albedo of 0.94 for freshly fallen snow which remains relatively constant as cloud cover increases. For c-Si PV systems the spectrally responsive albedo for snow and grass were found to be 0.87-0.91 and 0.24-0.154 respectively, as cloud cover increases. These values can be compared to the albedo predicted from spectral integration of 0.78 and 0.23 for snow and grass, respectively.

In addition, the relative effect of albedo on module power output was investigated, and was shown to be dependant on the ambient albedo, module angle, clearness ratio and geometric factor. In the two applications considered, with a snowy field on a clear day at a zenith angle of 48°, the power yield of a-Si:H PV system can be under-predicted by 1.6% or 7% for a 40° or 90° module angle, respectively. On a yearly basis, the use of improper albedo values can lead to an under-prediction of system yields of 0.04%, 2.4%, and 10.5% for systems at 25°, 40°, and 90° tilt from the horizontal, respectively. The results of this study have implications for proper systems evaluation and systems design, and lead to more research on tailoring PV technologies more specifically to the climate and geographic location where they are to be deployed.

6. Acknowledgements

References

Andrews, R.W., Pollard, A., Pearce, J.M., 2012. Improved parametric empirical determination of module short circuit current for modelling and optimization of solar photovoltaic systems. Solar Energy 86, 2240–2254.

ASTM, 2008. G173-03(2008) standard tables for reference solar spectral irradiances: Direct normal and hemispherical on 37 tilted surface.

Baldridge, A., Hook, S., Grove, C., Rivera, G., 2009. The ASTER spectral library version 2.0. Remote Sensing of Environment 113, 711–715.

Bamshad Houshyani, 2006. The effect of a varying solar spectrum on solar cells energy performance.

Barnard, J.C., Powell, D.M., 2002. A comparison between modeled and measured clear-sky radiative shortwave fluxes in arctic environments, with special emphasis on diffuse radiation. Journal of Geophysical Research 107, 10 PP.

Betts, T., Gottschalg, R., Infield, D., 2003a. ASPIRE - a tool to investigate spectral effects on PV device performance, in: Photovoltaic Energy Conversion, 2003. Proceedings of 3rd World Conference on, pp. 2182–2185 Vol.3.

Betts, T., Jardine, C., Gottschalg, R., Infield, D., Lane, K., 2003b. Impact of spectral effects on the electrical parameters of multijunction amorphous silicon cells, in: Photovoltaic Energy Conversion, 2003. Proceedings of 3rd World Conference on, pp. 1756–1759 Vol.2.

Carlson, D., Lin, G., Ganguly, G., 2000. Temperature dependence of amorphous silicon solar cell PV parameters, in: Photovoltaic Specialists Conference, 2000. Conference Record of the Twenty-Eighth IEEE, pp. 707–712.

Clough, S., Shephard, M., Mlawer, E., Delamere, J., Iacono, M., Cady-Pereira, K., Boukabara, S., Brown, P., 2005. Atmospheric radiative transfer modeling: a summary of the AER codes. Journal of Quantitative Spectroscopy and Radiative Transfer 91, 233–244.

Duffie, J.A., Beckman, W.A., 1991. Solar Engineering of Thermal Processes. Wiley-Interscience. 2 edition.

Gardner, A.S., Sharp, M.J., 2010. A review of snow and ice albedo and the development of a new physically based broadband albedo parameterization. Journal of Geophysical Research 115, 15 PP.

Goosse H., P.Y. Barriat, W. Lefebvre, M.F. Loutre, V. Zunz, 2011. Introduction to climate dynamics and climate modeling. http://www.climate.be/textbook.

Gottschalg, R., 2003. Experimental study of variations of the solar spectrum of relevance to thin film solar cells. Solar Energy Materials and Solar Cells 79, 527–537.

Gottschalg, R., Betts, T.R., Infield, D.G., Kearney, M.J., 2004. On the importance of considering the incident spectrum when measuring the outdoor performance of amorphous silicon photovoltaic devices. Measurement Science and Technology 15, 460–466.

Gueymard, C., 2001. Parameterized transmittance model for direct beam and circumsolar spectral irradiance. Solar Energy 71, 325–346.

Gueymard, C.A., 2005. Interdisciplinary applications of a versatile spectral solar irradiance model: A review. Energy 30, 1551–1576.

Gueymard, C.A., 2008. Prediction and validation of cloudless shortwave solar spectra incident on horizontal, tilted, or tracking surfaces. Solar Energy 82, 260–271.

Hirata, Y., Tani, T., 1995. Output variation of photovoltaic modules with environmental factors–i. the effect of spectral solar radiation on photovoltaic module output. Solar Energy 55, 463–468.

Houshyani, B., 2007. SEDES2 spectral model validation: A comparative study of spectral radiative transfer models for clear and cloudy sky conditions using SMARTS, SPCTRL2 and MODTRAN.

IEC, 2008. Photovoltaic devices - Part 7: Computation of the spectral mismatch correction for measurements of photovoltaic devices. Technical Report IEC 60904-7 ed3.0.

Jardine, C.N., Conibeer, G.J., Lane, K., 2001. PV-COMPARE: direct comparison of eleven PV technologies at two locations in northern and southern europe, in: Seventeenth EU PVSEC.

J.C Barnard, D.M Powell, 2001. Comparison of modeled and measured shortwave broadband radiative fluxes at the SGP and NSA sites (with special emphasis on diffuse radiation), in: Eleventh ARM Science Team Meeting Proceedings, Atlanta, Georgia.

Kenny, R.P., Ioannides, A., Mllejans, H., Zaaiman, W., Dunlop, E.D., 2006. Performance of thin film PV modules. Thin Solid Films 511-512, 663–672.

King, D., Hansen, B., 1991. A sensitivity analysis of the spectral mismatch correction procedure using wavelength-dependent error sources [solar cell testing]. Photovoltaic Specialists Conference, 1991. , 459–465 vol.1.

King, D.L., Boyson, W.E., Kratochvil, J.A., 2004. Photovoltaic array performance model. Sandia SAND2004-3535.

Martin, N., Ruiz, J., 2001. Calculation of the PV modules angular losses under field conditions by means of an analytical model. Solar Energy Materials and Solar Cells 70, 25–38.

Merten, J., Andreu, J., 1998. Clear separation of seasonal effects on the performance of amorphous silicon solar modules by outdoor I/V-measurements. Solar Energy Materials and Solar Cells 52, 11–25.

Nann, S., Emery, K., 1992. Spectral effects on PV-device rating. Solar Energy Materials and Solar Cells 27, 189–216.

Pathak, M., Pearce, J., Harrison, S., 2012. Effects on amorphous silicon photovoltaic performance from high-temperature annealing

pulses in photovoltaic thermal hybrid devices. Solar Energy Materials and Solar Cells 100, 199–203.

Pearce, J., Lau, A., 2002. Net energy analysis for sustainable energy production from silicon based solar cells, ASME. pp. 181–186.

Ricchiazzi, P., Yang, S., Gautier, C., Sowle, D., 1998. SBDART: a research and teaching software tool for plane-parallel radiative transfer in the earths atmosphere. Bulletin of the American Meteorological Society 79, pp. 2101–2114.

Rther, R., Kleiss, G., Reiche, K., 2002. Spectral effects on amorphous silicon solar module fill factors. Solar Energy Materials and Solar Cells 71, 375–385.

Rther, R., Livingstone, J., 1995. Seasonal variations in amorphous silicon solar module outputs and thin film characteristics. Solar Energy Materials and Solar Cells 36, 29–43.

Schwabe, U., Jansson, P., 2009. Performance measurement of amorphous and monocrystalline silicon PV modules in eastern U.S. energy production versus ambient and module temperature, in: Instrumentation and Measurement Technology Conference, 2009. I2MTC '09. IEEE, pp. 1636–1641.

Simon, M., Meyer, E.L., 2011. The effects of spectral evaluation of c-si modules. Progress in Photovoltaics: Research and Applications 19, 1–10.

Thevenard, D., Driesse, A., Turcotte, D., Poissant, Y., 2010. Uncertainty in Long-Term Photovoltaic Yield Predictions. Technical Report 2010-122 (RP-TEC) 411-IEARES. CanmetENERGY, Natural Resources Canada.

Tselioudis, G., Rossow, W.B., Rind, D., 1992. Global patterns of cloud optical thickness variation with temperature. Journal of Climate 5, 1484–1495.

Warren, S.G., 1972. Optical properties of snow. Reviews of Geophysics 20, PP. 67–89.

Whitaker, C.M., Newmiller, J.D., 1998. Photovoltaic module energy rating procedure. Final subcontract report. Technical Report NREL/SR-520-23942. NREL.

Williams, S., Gottschalg, R., Infield, D., 2003. Performance of photovoltaic modules in a temperate maritime climate, in: Photovoltaic Energy Conversion, 2003. Proceedings of 3rd World Conference on, pp. 2070–2073 Vol.2.

Wiscombe, W.J., Warren, S.G., 1980. A model for the spectral albedo of snow. i: Pure snow. Journal of the Atmospheric Sciences 37, 2712–2733.